

Constitutive relations for numerical analysis of stressdeformation behavior of concrete subjected to thermal loads

V.Mechtcherine & H.S.Müller
University of Karlsruhe, Karlsruhe, Germany

ABSTRACT: On the basis of foregoing experimental and the numerical investigations a simple and an advanced material law for concrete under thermal load were developed. The advanced material law is based on a rheological-statistical, physically sound material model, whereas the constitutive relations of the simple material law are purely empirical. Further, a procedure to take into account the heterogeneity of concrete throughout the structure was developed. The simple material law was verified by the simulation of the bend tests, which had been performed at different temperatures. Afterwards it was used for a numerical prediction of the cracking behavior of a concrete slab subjected to a sudden cooling. The obtained results were checked by means of full-scale experiments.

1 INTRODUCTION

In practice the majority of concrete structures are exposed to the ambient environment or service conditions resulting in more or less severe temperature changes. The existing codes and guidelines generally consider only the linear components of the stresses induced by the temperature fluctuations and neglect the eigenstresses caused by the non-linearity of the corresponding temperature distributions. The main reasons are evidently the lack of a general analytical solution algorithm to calculate the eigenstresses induced by such distributions and the difficulty to predict the damage evolution (crack development) caused by highly non-linear temperature fields. Consequently, for concrete members under thermal load a numerical analysis has to be performed in order to allow the prediction of the eigenstresses and the related consequences. This requires both, a better knowledge of the fracture mechanical behavior of concrete under such conditions and a suitable algorithm for the numerical calculations.

Thermal shock is the most severe case of loading induced by weather changes. In foregoing studies the temperature distribution in a concrete slab initially heated by sunshine and subsequently cooled by a sudden rain and hail was investigated by means of the FE method (Mechtcherine 2000). The numerical analysis of the temperature distribution and the corresponding thermal deformations in the slab during the thermal load provided parameters, in particular temperature and strain rates for a subsequent

experimental investigation on concrete specimens. From the gained test data the characteristics of the material response, i.e. uniaxial tensile strength f_t , modulus of elasticity E_0 and fracture energy G_F were evaluated for two ordinary concretes with w/c -ratios of 0.45 and 0.6, respectively (Mechtcherine et al. 1995). In addition, numerical calculations were performed considering specimens with the same geometries as used in the actual tests. In order to take into account the heterogeneity of the concrete, different calculation methods within the frame of the smeared crack concept were investigated (Mechtcherine & Müller 2000).

In this paper a "simple" and an "advanced" material law for concrete under thermal load are developed on the basis of the results obtained from the experimental and numerical investigations.

2 MATERIAL LAWS FOR CONCRETE UNDER THERMAL LOAD

For the development of the constitutive relations to describe the fracture behavior of concrete under consideration of the effects of temperature and strain rate as observed in the experiments (Mechtcherine et al. 1995) two different approaches were chosen. The "simple material law" should imply constitutive relations, which have a simple mathematical formulation and which are purely empirical. The "advanced material law" on the other hand should be based on a rheological-statistical, physically sound material model.

Both material laws, the “simple” and the “advanced”, were formulated within the frame of the cohesive crack type models (Hillerborg et al. 1976, Bažant & Oh 1983). Further, for both material laws a linear σ - ε -relation was used to represent the stress-strain behavior of the material outside the crack region. It is defined by the tensile strength f_t and the modulus of elasticity E_0 (see Figure 1 and Figure 7). For the crack region however very different stress-crack opening formulations were chosen.

2.1 Simple material law

In the “simple” material law the stress-crack opening relation for uniaxial tension was described as a bi-linear curve (see Fig. 1). Following the test results, the characteristic “knee” of the σ - w relation was defined to be at a tensile stress $\sigma_{ct} = 0.7$ MPa for all loading conditions. The area under the complete stress-crack opening curve corresponds to the fracture energy G_F obtained from the uniaxial tension tests. The area under the first, steeper part of the descending branch extrapolated to the stress $\sigma = 0$ (at a crack opening w_{cr1} , compare Fig. 1) is defined as specific crack formation energy G_{FI} . This value was derived by means of a numerical analysis of the fracture mechanical experiments (Mechtcherine 2000). The characteristic values w_1 (crack opening at the “knee” of the σ - w relation) and w_{cr} (crack opening at which no tensile stresses can be transmitted any more) can be calculated using Equations 1 and 2:

$$w_1 = \frac{2 \cdot G_{FI} \cdot (f_t - \sigma_{ct})}{f_t^2} \quad (1)$$

$$w_{cr} = 2 \cdot \left(\frac{G_F - G_{FI}}{\sigma_{ct}} + \frac{G_{FI}}{f_t} \right) \quad (2)$$

In the crack band model the critical strain ε_{cr} and the strain ε_1 depend on the characteristic element length h and can be calculated from the corresponding crack openings using following formulas: $\varepsilon_{cr} = w_{cr}/h$ and $\varepsilon_1 = w_1/h$. Accordingly, the area under the entire σ - ε relation is equal to G_F/h , while the area

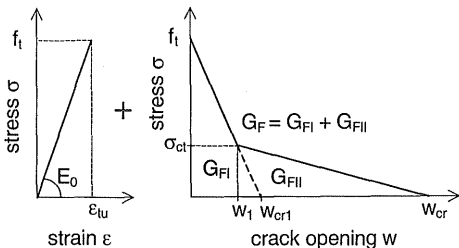


Figure 1. The fictitious crack model by Hillerborg et al. (1976) for the description of the behavior of concrete subjected to tension

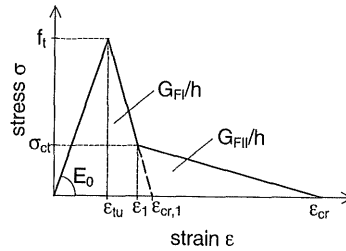


Figure 2. The crack band model by Bažant & Oh (1983) for the description of the behavior of concrete subjected to tension

marked off by the first, steeper part of the descending branch of the σ - ε relation is equal to G_{FI}/h (Fig. 2).

In order to derive the functional dependence of the fracture mechanical parameters from the temperature and strain rate the experimental data obtained from uniaxial tensile tests were analyzed using different regression functions. This analysis showed that for the both concretes investigated by Mechtcherine et al. (1995) there are nearly linear relations between the f_t -, E_0 - and G_{FI} -values on one hand and the temperature on the other hand (Fig. 3 gives an example for the effect of the temperature on the tensile strength of concrete at three different strain rates). Further, it was found that the logarithmic regression could describe best the relations between the f_t -, E_0 - and G_{FI} -values and the strain rate.

On the basis of the analysis of the experimental and numerical findings Equations 3-5 were developed to describe the functional dependence of the f_t -, E_0 - and G_{FI} -values from the temperature and strain rate. Using these equations average values of the fracture mechanical parameters can be calculated for the temperature ϑ and strain rate $\dot{\varepsilon}$ from the corresponding material parameters $f_{t,0}$, $E_{0,0}$ or $G_{FI,0}$, which have been de-

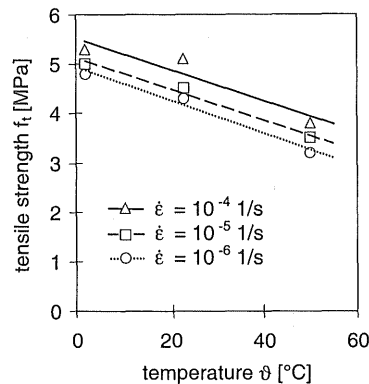


Figure 3. Effect of the temperature on the tensile strength f_t and the corresponding regression lines for the concrete with $w/c = 0.45$

terminated experimentally for a reference temperature ϑ_0 at a reference strain rate $\dot{\epsilon}_0$:

$$f_t = a_{f_t} \cdot f_{t,0} + b_{f_t} \cdot (\vartheta_0 - \vartheta) + c_{f_t} \cdot \log\left(\frac{\dot{\epsilon}}{\dot{\epsilon}_0}\right) \quad (3)$$

$$E_0 = a_{E_0} \cdot E_{0,0} + b_{E_0} \cdot (\vartheta_0 - \vartheta) + c_{E_0} \cdot \log\left(\frac{\dot{\epsilon}}{\dot{\epsilon}_0}\right) \quad (4)$$

$$G_{FI} = G_{FI,0} + b_{G_{FI}} \cdot (\vartheta_0 - \vartheta) + c_{G_{FI}} \cdot \log\left(\frac{\dot{\epsilon}}{\dot{\epsilon}_0}\right) \quad (5)$$

where a_{par} , b_{par} and c_{par} are coefficients depending on the concrete composition. They were determined experimentally for the corresponding material parameters f_t , E_0 or G_{FI} . Table 1 gives the values of the coefficients a , b and c for the both investigated concretes.

Table 1. Values of the coefficients a , b and c in Equations 3-5

Concrete (w/c)	Material parameter	Coefficient		
		a	b	c
0.45	f_t	0.943	0.0324	0.317
		[-]	[MPa/K]	[MPa]
	E_0	0.973	0.0742	0.842
		[-]	[GPa/K]	[GPa]
	G_{FI}	-	0.159	7.23
			[N/(m·K)]	[N/m]
0.6	f_t	0.928	0.0241	0.417
		[-]	[MPa/K]	[MPa]
	E_0	0.983	0.0393	1.303
		[-]	[GPa/K]	[GPa]
	G_{FI}	-	0.083	8.34
			[N/(m·K)]	[N/m]

Figure 4 shows as an example the stress-strain and stress-crack opening relations for temperatures of 2 °C and 50 °C at a strain rate of 10^{-6} 1/s determined from Equations 1-5 for the concrete with w/c = 0.45. As a whole, the material law curves agree with the corresponding relations obtained from the uniaxial tension tests reasonably well. However, the stress-strain relation acc. to this simple material law do not reproduce the derivation of the measured σ - ϵ curves from the linearity, as it had been observed in the tests on unnotched specimens. This derivation is caused partly by the development of cracks in concrete prior to reaching of the tensile strength, which is a material phenomenon, partly by some quasi-structural phenomena like a plain stress condition on the edges of specimen, by the “wall-effect” or by some inevitable eccentricity of loading. The concrete damage due to the crack growth prior to reaching the tensile strength was considered in the formulation of the “advanced material law” (see section 2.2).

With regard to the comparison of the developed stress-crack opening relations and the σ - w curves obtained from the uniaxial tension tests on notched prisms, it should be pointed out, that the difference between the developed and the measured σ - w relations concerning the starting points on the ordinate axis is due to the reduction of the tensile strength caused by the stress concentration on the notches of the concrete prisms in the experiment. On the other hand the σ - w relations acc. to the simple material law start always at the value of the tensile strength acc. to Equation 3, which was obtained by evaluation of the results of the tests on unnotched specimens.

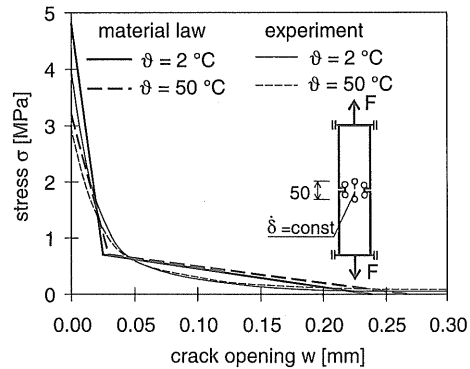
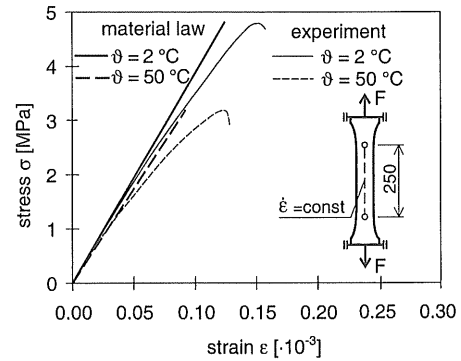


Figure 4. Stress-strain (above) and stress-crack opening (below) relations acc. to the simple material law and the corresponding curves obtained experimentally for the concrete with w/c = 0.45 at the temperatures of 2 °C and 50 °C at a strain rate of 10^{-6} 1/s

2.2 Advanced material law

In general the “advanced” material law, to be termed as rheological material law, had to meet the same basic requirements concerning its unproblematic implementation in the various types of the cohesive crack model and the consideration of the effects of the temperature and strain rate on the fracture mechanical properties of concrete as the simple material law. However, by developing the advanced material law some additional features were strived for.

First, it should be based on a clear and physically sound material model, which should take into account the decisive mechanisms of concrete fracture. Further, the new material law should allow to describe the damage of concrete before and after the tensile strength is reached. Finally, the constitutive relations should provide non-linear curves with a steady transition from the ascending to the descending branch of the stress-strain relation.

The material model for the rheological material law was developed using a rheological-statistical approach. As basic rheological elements of the model spring elements were used to represent the elastic behavior of concrete, while friction elements were chosen to describe the non-elastic behavior (see Fig. 5, above). All elements of both groups were arranged parallel (see Fig. 5, below).

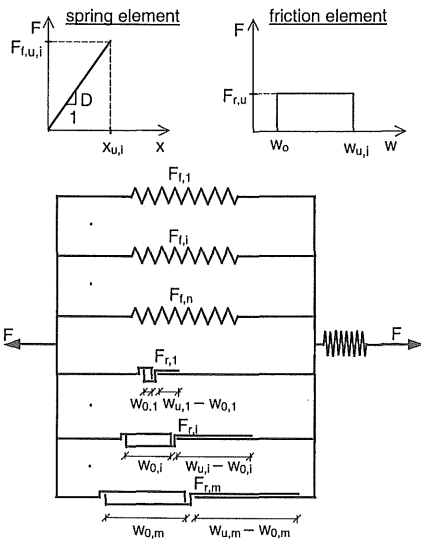


Figure 5. Rheological material model: basic elements and their functions (above), the principal arrangement of the elements in the model (below)

At the beginning of loading all spring elements are active. Each spring element has a different strength $F_{t,u,i}$, so that the $F_{t,u,i}$ -values follow the chosen statistical function. As a result, with an increasing load the spring elements fail one after the other, in order of their $F_{t,u,i}$ -values. The failure of the individual elements, which represents the increasing damage of concrete, leads to a reduction of the stiffness of the entire system. The deformation resulting from the reduction of the stiffness is considered as a part of the crack opening.

In contrast to the spring elements all friction elements are inactive at the beginning of loading. Before each friction element an additional aid element is placed, which can be stretched remaining un-

stressed up to a definitive, for each element different crack opening $w_{0,i}$. With increasing load and as a result of the failure of spring elements the deformability of the individual aid elements is consumed so that the corresponding friction elements become active. Each friction element can transfer a force $F_{r,u}$, before it fails at a crack opening $w_{u,i}$.

The behavior of the model as a whole is governed by statistical rules. It was assumed, that the strength of the spring elements varies acc. to the theory of Weibull (1939). Therefore, the Weibull distribution was defined to be the failure function of the spring elements (Equation 6):

$$f(x) = \frac{\gamma}{\beta} \cdot \left(\frac{x - \alpha}{\beta} \right)^{\gamma-1} \cdot e^{-\left(\frac{x - \alpha}{\beta} \right)^{\gamma}} \quad (6)$$

where x = random variable; here the crack opening w in concrete was assumed as a decisive control parameter for this variable. The coefficients $\alpha, \beta (> 0)$ and $\gamma (> 0)$ give position, scale and shape of the function, respectively. On the basis of Equation 6 functions for the number of the still intact spring elements n_t , the number of the failed spring elements \bar{n}_f as well as for the probability of the failure of the spring elements $\frac{d\bar{n}_f}{dw}$ in dependence on the crack opening w could be derived (the equations and the corresponding graphs are given in Fig. 6, the details may be found in Mechtcherine 2000).

With increasing deformation resp. crack opening more and more spring elements fail, and more and

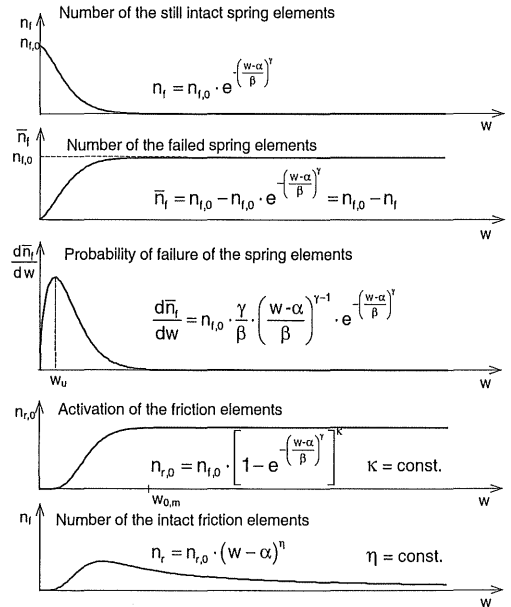


Figure 6. Graphs and equations for the number of the spring and friction elements as functions of the crack opening, with $\alpha = 0$

more friction elements become active. The equation for the number of the activated friction elements $n_{r,0}$ and the corresponding graph are given in Figure 6 as well. For the description of the failure of the friction elements a power function was chosen. The number of the still intact friction elements n_f can be calculated multiplying this function by the number of the activated friction elements $n_{r,0}$ (see the equation and the corresponding graph in Fig. 6, below).

For the derivation of a constitutive relation from the statistical equations given in Figure 6 it was assumed that the tensile strength of the model and the corresponding non-linear deformation (here: the ultimate crack opening w_u) are reached, when the probability of failure of the spring elements is the highest. Consequently, the tensile stress $\sigma_r(w)$ taken up by the spring elements is proportional to the probability of failure of the spring elements \bar{n}_r/dw . On the other hand, the stress $\sigma_f(w)$ taken up by the friction elements is proportional to the number of the intact friction elements n_f . The stress $\sigma(w)$, which can be taken up by the model as a whole adds up from the load carrying capacities of the both element groups acc. to Equation 7:

$$\sigma(w) = \sigma_r(w) + \sigma_f(w) \quad (7)$$

$$= A \cdot \frac{\gamma}{\beta} \cdot \left(\frac{w-\alpha}{\beta}\right)^{\gamma-1} \cdot e^{-\left(\frac{w-\alpha}{\beta}\right)^\gamma} + B \cdot \left[1 - e^{-\left(\frac{w-\alpha}{\beta}\right)^\kappa}\right] \cdot (w-\alpha)^\eta$$

where A and B are correlation coefficients.

Figure 7 shows the stress-strain and stress-crack opening relations resulting from the material model. The σ - ε relation is defined by the elastic properties of the spring introduced serially to the rest of the model. It can be described by the Hooke's law. The σ - w diagram in Figure 7 presents the σ - w relation for the entire model as well as the corresponding curves for the individual groups of elements.

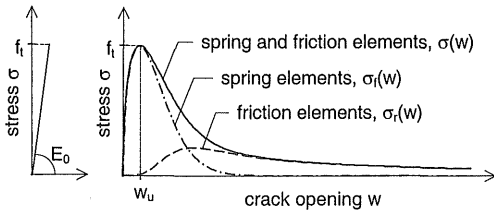


Figure 7. Schematic view of the stress-strain and stress-crack opening relations resulting from the rheological material model

In order to proceed from the basic material model towards the material law for concrete subjected to thermal loads the coefficients of the model, i.e. those of Equation 7 must be fixed in the manner, that the fracture behavior of concrete could be described correctly for different temperatures and strain rates. Equation 7 has seven unknowns – α , β , γ , κ , η , A

and B – which have to be defined. Therefore, it would be best to have a system of seven equations to determine all unknowns directly. However, on the basis of Equation 7 a system of only three equations could be derived, see Equations 8-10:

$$f_t = \sigma(w_u) \quad (8)$$

$$\frac{d\sigma(w)}{dw} = 0 \text{ bei } w = w_u \quad (9)$$

$$G_F = \int_0^{w_{cr}} \sigma(w) dw \quad (10)$$

where $w_{cr} = 0.5$ mm, representing the maximum crack opening observed in the experiments.

In order to find out, which 3 unknowns have to be determined by solving this system of equations, an extensive parameter study was performed. Analyzing the results of this study the coefficients β , γ and B were found to be most suitable for the adjustment of the stress-crack opening relation acc. to Equation 7 on the basis of experimental results. The other four coefficients were defined as constants. The following values were assigned: $\alpha = 0$, $\kappa = 4$, $\eta = -1$ and $A = 0.04$.

The values of the ultimate crack opening w_u were calculated from the results of the uniaxial tension tests on unnotched specimens using Equation 11:

$$w_u = C \cdot \left(\varepsilon_{tu} - \frac{f_t}{E_0} \right) \cdot l_{mes} \quad (11)$$

where ε_{tu} = ultimate strain acc. to Equation 12 and l_{mes} = gauge length (for the own tension tests: $l_{mes} = 250$ mm). The coefficient C ($0 \leq C \leq 1$) was introduced in order to consider the phenomena like the “wall effect” or the effect of the possible eccentricity of loading, which in fact contribute to the non-linearity of the stress-strain relation, however they are not characteristic for the behavior of concrete itself. The ultimate strain ε_{tu} can be estimated using Equation 12. The statistical evaluation of the experimental results showed that the effect of the temperature and the strain rate on this material parameter could be described using the same approach as it had been used for $f_{t,r}$, E_0 and G_{FI} -values:

$$\varepsilon_{tu} = a_{\varepsilon_{tu}} \cdot \varepsilon_{tu,0} + b_{\varepsilon_{tu}} \cdot (\vartheta_0 - \vartheta) + c_{\varepsilon_{tu}} \cdot \log\left(\frac{\dot{\varepsilon}}{\dot{\varepsilon}_0}\right) \quad (12)$$

where $\varepsilon_{tu,0}$ is the ultimate strain determined experimentally for a reference temperature ϑ_0 at a reference strain rate $\dot{\varepsilon}_0$; a, b and c are coefficients obtained by the evaluation of the test results by means of a regression analysis. These coefficients for both investigated concretes are given in Table 2.

The parameter analysis performed using the sketched algorithm proved that by applying the cho-

Table 2. Values of the coefficients a, b and c in Equation 12

Concrete (w/c)	Coefficients		
	a [-]	b [10^{-6} 1/K]	c [10^{-6}]
0.45	0.960	0.498	6.45
0.6	0.954	0.486	10.36

sen approach the material laws can be derived for all parameter combinations investigated in the experimental studies. In order to compare the calculated and the experimental curves directly the crack opening $w < w_{ts}$, which occurs before the tensile strength f_t is reached, was considered in the material law when drawing the σ - ε curve by using Equation 13:

$$\varepsilon = \varepsilon_{el} + \frac{w}{l_{mes}} \quad (13)$$

where ε_{el} = elastic part of the strain, l_{mes} = gauge length in the uniaxial tension tests on unnotched specimens (here: $l_{mes} = 250$ mm).

On the other hand, concerning the stress-crack opening curves acc. to the material law only the de-

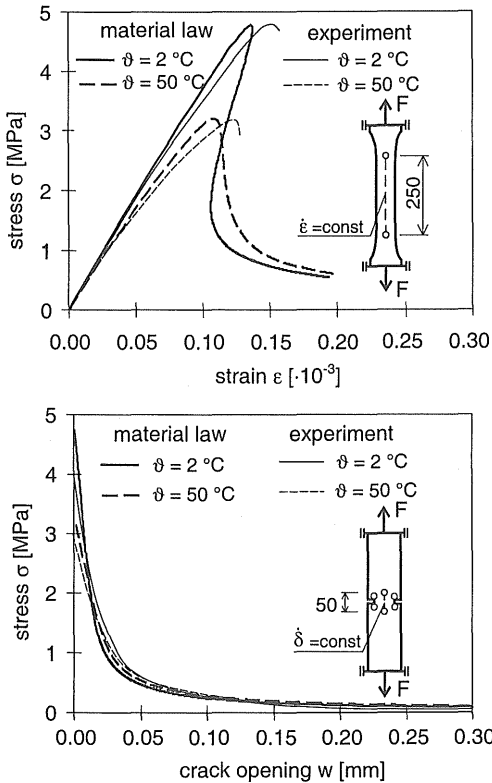


Figure 8. Stress-strain (above) and stress-crack opening (below) relations acc. to the rheological material law and the corresponding curves obtained experimentally for the concrete with $w/c = 0.45$ at the temperatures of 2°C and 50°C at a strain rate of 10^{-6} 1/s (with $C = 0.5$)

scending branch were considered. This enabled a better comparison with the corresponding relations obtained from the tests on notched specimens.

Figure 8 shows as an example stress-strain and stress-crack opening relations for the temperatures of 2°C and 50°C at a strain rate of 10^{-6} 1/s determined acc. to the rheological material law as well as the corresponding relations obtained experimentally for the concrete with $w/c = 0.45$. The predicted relations provide a good agreement with the measured curves.

2.3 Consideration of the heterogeneity of concrete

The first numerical analysis of a concrete slab under thermal shock using the described material laws led to the result, that in case of a uniform thermal load acting over the entire upper surface of the slab strains larger than the failure strain $\varepsilon_{tu,0} = f_{t,0}/E_{0,0}$ arise in all elements of the slab surface, irrespective of the fineness of FE discretisation. Therefore, in each element one or several „cracks“ develop and all these „cracks“ grow in the same way towards the interior of the slab. Hence, no information could be obtained on the quantity, periodicity and development of cracks. To obtain this information, the heterogeneity of concrete, which is usually neglected in comparable analyses, must be considered.

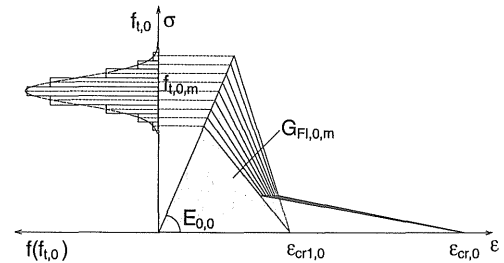


Figure 9. Assignment of the constitutive relations of the simple material law to the groups of finite elements

The heterogeneity was introduced considering the tensile strength $f_{t,0}$ to be an independent random variable following a Gaussian distribution (see Fig. 9). The modulus of elasticity $E_{0,0}$ as well as the critical strains $\varepsilon_{cr,0}$ and $\varepsilon_{cr1,0}$ were kept constant for all finite elements. The reference values of the fracture energy $G_{F,0}$ resp. the crack formation energy $G_{F1,0}$ were related to the corresponding $f_{t,0}$ -values by the following formulas: $G_{F,0} = f_{t,0} \cdot w_{cr,0}/2$ and $G_{F1,0} = f_{t,0} \cdot w_{cr1,0}/2$. For a better handling, the elements were subdivided into nine groups according to their tensile strength. To each group its own material law was assigned. Details may be found in (Mechtcherine 2000).

3 VERIFICATION OF THE MATERIAL LAWS

In order to assess the quality of the developed material laws a comparison of calculated predicted results and the results of the experiments, which had not been considered for the derivation of the constitutive relations, were performed. In the following the verification of the simple material law is presented, which was carried out using own bend tests and full-scale experiments on concrete slabs as references.

3.1 Simulation of the bend tests

First, own three-point bend tests performed at different temperatures were considered. In these tests the load was applied from below in order to compensate the dead weight. The FE discretization of the beam specimens and the boundary conditions are shown in Figure 10. Figure 10 presents also the calculated load-deflection diagrams for the concrete with $w/c = 0.45$ at the temperatures of $2\text{ }^{\circ}\text{C}$ and $50\text{ }^{\circ}\text{C}$ as well as the corresponding measured curves. The simulation using the simple material law provided a very good prediction of the concrete behavior observed experimentally (Fig. 10).

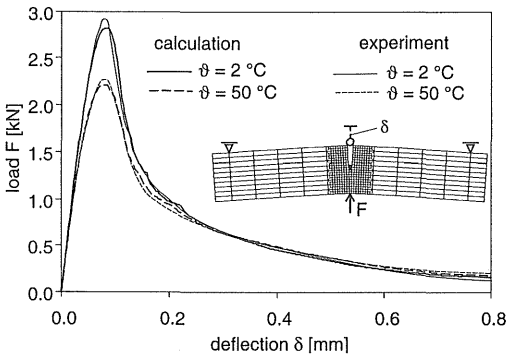


Figure 10. Calculated and measured load-deflection diagrams for the concrete with $w/c = 0.45$ at different temperatures

3.2 Crack development in a concrete slab subjected to thermal shock

For a further verification the simple material law modified by the stochastic approach as described in Section 2.3 was applied in a FE analysis of the damage evolution in a concrete slab subjected to thermal shock. Foremost, preliminary numerical investigations were performed to study the effect of the intensity of thermal load and the slab geometry on the deformation and cracking behavior of concrete. As a result, the cracks induced by thermal shock in thicker slabs were deeper as those in the thinner slabs. This tendency was valid up to a slab thickness of approx. 600 mm. The minimal representative

length of the structural member required for a reliable analysis of the periodicity of cracks was estimated by means of the FE analysis as well.

Based on the numerical analysis a concrete slab with the length of 2000 mm, the width of 800 mm and the thickness of 660 mm was chosen for full-scale experiments (Fig. 11). The preliminary numerical investigations showed furthermore, that due to thermal shock numerous fine cracks will develop (crack openings at the surface of approximately $0.02 - 0.05\text{ mm}$), while their location could not be foreseen. This finding showed the difficulty to quantify the opening of such cracks in an experiment. Because of that, a 15 mm deep notch was introduced in the middle of the slab to enable the permanent measurement of the opening of this pre-existing "crack".

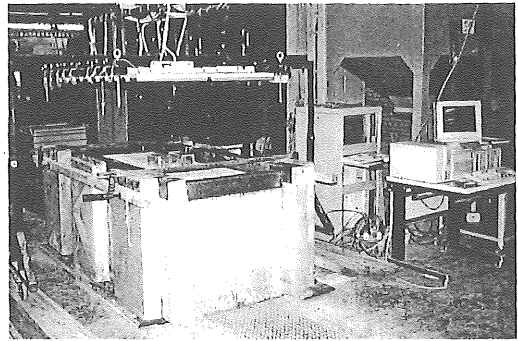


Figure 11. Set-up of the full-scale experiments

The numerical calculations, assuming an usual sunshine intensity, provided for normal weight concretes maximum temperatures at the upper slab side of approximately $50\text{ }^{\circ}\text{C}$, and showed no dramatic crack development as a result of the following sudden cooling (Mechtcherine 2000). For this reason, for the full-size tests a more severe heating of the concrete slab up to a surface temperature of $80\text{ }^{\circ}\text{C}$ was chosen in order to induce higher thermal gradients during the cooling phase and, hereby, to be on the safe side when assessing the possible damage of the concrete members exposed to sudden weather changes.

In the experiments the concrete slab was heated six hours by means of twenty infrared lamps with an entire radiation intensity of approx. 1350 W/m^2 . Subsequently, the upper surface of the slab was cooled for 50 min by an ice-water mixture with a temperature of $4\text{ }^{\circ}\text{C}$. To achieve an uniform propagation of the temperature front toward the interior of the slab, its side areas were insulated by thick glass wool platens (see Fig. 11). The temperature was measured by thermocouples throughout the vertical cross-section of the slab.

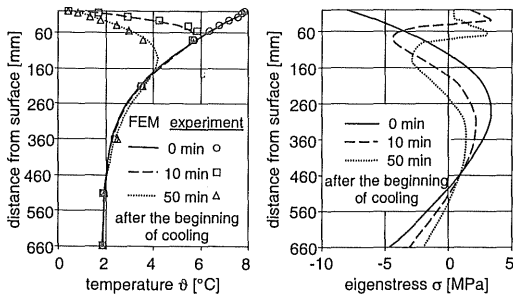


Figure 12. Calculated and measured temperature distributions over the distance from the slab surface after six hours of heating and following sudden cooling (left); calculated distributions of the main stresses (parallel to the length of the slab) over the distance from the slab surface for different times after the beginning of cooling (right)

Parallel to the experiments numerical simulations were performed. In the FE analysis the slab was modeled by a mesh with an element length of 10 mm. Since a one-point integration scheme was applied, the characteristic length of the finite elements h corresponded to the side length of the elements. The calculated and measured temperature distributions in the slab just before cooling as well as 10 and 50 minutes after the beginning of cooling are shown in Figure 12 (left). Due to the sudden temperature change high thermal gradients arise, which lead to considerable eigenstresses. When reaching the tensile strength of the concrete these eigenstresses cause the formation of fine surface cracks. Due to the sustained cooling the cracks propagate – following the propagation of the cold front – toward the interior of the slab. Figure 12 (right) shows the calculated distribution of stresses over the distance from the cooled surface for the vertical cross-section where a crack develops. The position of this cross-section is marked in Figure 13 by an arrow.

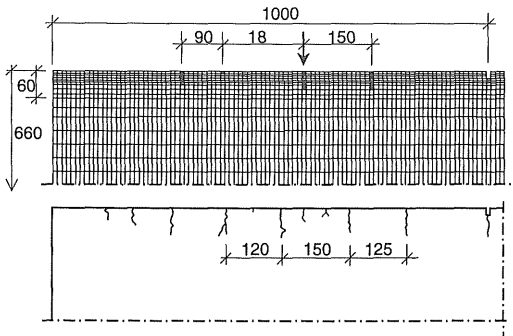


Figure 13. Distribution of the strains $\epsilon \geq 3 \cdot 10^{-4}$ over the concrete slab after 50 minutes of cooling (above) and the typical crack pattern observed in the full-scale experiments: side view of one half of the concrete slab (below)

The distribution of strains $\epsilon \geq 3 \cdot 10^{-4}$ over the concrete slab after 50 minutes of cooling gives information about the distribution, depths and widths of cracks caused by the thermal shock (Fig. 13, above). The crack widths at the surface of approx. 0.05 mm, the crack depths up to 50 - 60 mm and the distances between two larger neighbor cracks of approx. 90 - 180 mm are typical results of the numerical simulations. The crack pattern obtained in the full-scale tests (Fig. 13, below) corresponds very well to the numerically predicted crack pattern. The crack widths measured in the experiments are also in a good agreement with the calculated crack openings.

4 SUMMARY

On the basis of the experimental and the numerical investigations a “simple” and an “advanced” material law for concrete subjected to thermal load were developed. The advanced material law is based on a rheological-statistical, physically sound material model, whereas the constitutive relations of the simple material law are purely empirical.

The simple material law was verified by the simulation of the bend tests, which had been performed at different temperatures. Further, it was used for a numerical prediction of the cracking behavior of a concrete slab subjected to thermal shock. To verify the results of the simulation full scale experiments were performed. The results of the experiments concerning the temperature distribution as well as the quantity, the periodicity and the development of cracks were found to be in a good agreement with the predictions by the numerical analysis.

5 REFERENCES

- Bažant, Z.P. & Oh, B.H. 1983. Crack band theory for fracture of concrete. *Materials and Structures* 16 (93): 155-177.
- Hillerborg, A., Modér, M. & Petersson, P.-E.. 1976. Analysis of crack formation and crack growth in concrete by means of fracture mechanics and finite elements. *Cement and Concrete Research* 6 (6): 773-782.
- Mechtcherine, V. 2000. *Investigations on crack spreading in concrete*. Doctoral thesis, University of Karlsruhe, in German.
- Mechtcherine, V., Garrecht, H. & Hilsdorf, H.K. 1995. Effect of temperature and loading rate on fracture behaviour of concrete subjected to uniaxial tension. In F.H. Wittmann (ed.), *Fracture Mechanics of Concrete Structures*: 719-728. Freiburg: Aedificatio Publishers.
- Mechtcherine, V. & Müller, H.S. 2000. A stochastic type continuum model for analysis of fracture behaviour of cementitious materials. In A.M. Brand, V.C. Li and I.H. Marshall (eds), *Brittle Matrix Composites*: 241-250. Cambridge: Woodhead Publishing Ltd.
- Weibull, W. 1939. A statistical theory of the strength of materials. *Ingenjör Vetenskaps Akademiens (The Royal Swedish Institute for Engineering Research)* 151: 1-45.